Design and Analysis of Small-Scale Vertical Axis Wind Turbine

Xiaona Ji*, Jörg Schlüter [†]

**Corresponding author,E-mail: ji0002na@ntu.edu.sg*
School of Mechanical and Aerospace Engineering
Nanyang Technological Univeristy, Singapore

Keywords: Low speed wind tunnel, Vertical-axis wind turbine, Aerodynamics, Performance coefficient.

Abstract

This study presents a combined experimental, computational and theoretical study of the aerodynamic performance of a small scale straight bladed vertical axis wind turbine (SB-VAWT). The wind tunnel tests were carried out to study the overall performance of the turbine using three different airfoil profiles. It is shown experimentally that blade profile has significant effect on its performance. Unsteady-flow computations were performed helping to understand the aerodynamics of the turbines' performance. The two- and three- dimensional unsteady flow field simulation around the turbines were performed using time accurate Reynolds Averaged Navier Stokes (RANS) solver. Interesting features about the dynamic stall around the blades and the interaction of the blade wakes with the following blades were observed. Comparisons of the 2D and 3D simulations highlight the strong 3D effects, including the blade tip vortices and effects. Wind tunnel measurements were carried out at low tip-speed ratios (TSRs) to study the self-starting capability initially, while a motor was used to study the full range of TSR performance of small scale turbine model. Comparisons of the overall turbine performance coefficient have been studied through wind tunnel measurements, simulations and theoretical analysis. Significant tunnel wall effects were observed from simulation results and strongly influence the overall performance results.

1 Introduction

As the demand for renewable energy grows, the use of small wind turbines in urban areas is increasingly attractive. The simple straight-bladed Darrieus type vertical axis wind turbine (SB-VAWT) has gained attention due to its simple blade design. As the maximum possible efficiency of lift driven turbines is larger than for drag driven turbines, the main attention nowadays is focussed on lift driven turbines.

Horizontal Axis Wind Turbine (HAWT) designs are highly optimized and widely used in all current large scale wind farms due to its good self-starting characteristics at low wind speeds. However, HAWT have the disadvantages that they have to be positioned perpendicular to the wind direction and hence have difficulties to adjust to fast changing direction. VAWT have the advantage that they are independent of wind direction for their operations. The majority of research on VAWT design was carried out as long ago as the late 1970s and early 1980s, notably at the USA department of Energy Sandia National Laboratories and in UK by Reading University, and VAWT Ltd., who erected several prototypes including a 500kW at Carmarthen Bay. Extensive research projects were carried out in the UK to investigate the potential of fixed pitch H-rotor VAWT for large scale power generation.

Generally, VAWTs have poor self-starting torque due to the blade stall condition at high angle of attack, although the H-rotor has better self-starting ability than the Darrieus curved bladed turbine [1]. The blades are straight and therefore the radius is equal over the whole length of the blade. The power is now generated over the complete length of the blade. The blade can be swept in a helical manner to disperse the moment forces on the axis over a larger angle. The blades of a VAWT have to develop lift and must have sufficient thickness to withstand the loads. For a grid connected turbine, the grid can be used to start the turbine by using the generator as a motor [2] and therefore the self-starting is not a major issue. For a HAWT, the power coefficient /performance coefficient C_p value is usually between 0.40 and 0.50 [3], close to the Betz limit. However, it is difficult to generalize a typical C_p for VAWTs because there are many different designs. Musgrove has shown that VAWTs have efficiencies comparable with the best modern HAWT through his extensive experimental and theoretical studies in 1987[4]. Comparisons of power performance between H-rotor Darrieus and HAWT have been carried out based on the existing data from Sandia National Laboratories and National Renewable Energy laboratory. Investigation shows that the turbines operate at different optimum tip speed ratios and the Darrieus turbine is known to have a lower C_p than HAWT. However, Paraschivoiu claim that the gap of C_p between Darrieus and HAWT is not large and that the performance can be improved by change in airfoil design.

The application of Computational Fluid Dynamics (CFD) techniques for VAWT is an emerging subject. Considerable improvements in the understanding of VAWT can be achieved through the use of CFD and experimental measurements. It is known that VAWT exhibit complex unsteady aerodynamics. A rapid change in angle of attack and the resultant wind velocity result in the phenomenon that different Reynolds number are experienced as blade rotate, which leads to the dynamic stall phenomenon. Previous research performed by Fujisawa et al. [5] and McCroskey et

al. [6] revealed complex mechanisms of dynamic stall, in which two counter-rotating vortices being generated and transported in the wake. Several studies relating to the detailed flow field and aerodynamic prediction of VAWT have been performed previously. In a research carried out by Brahimi et al [7] in 1995, a computational code called "Tkelow' was developed to perform 2D incompressible unsteady flow simulation on Darrieus-type VAWT, including prediction of the dynamic stall. More recently Hwang et al. [8] employed a commercial CFD package, STAR-CD with moving mesh and k-ϵ high Reynolds turbulence model. Investigation on actively controlling blade pitch angles was performed. However no detailed flow field studies were made.

The motivation for the current research is to get better understanding of self-starting capability on the characteristic of VAWT. The focus of present paper is to illustrate some of the improved understanding of the aerodynamics of vertical axis wind turbine performance through wind tunnel testing, finite phase step analysis studied with Microsoft Excel and computational simulation performed with Fluent.

2 VAWT Aerodynamic Study

This section illustrates the theoretical background performed in finite phase step analysis. We have developed a Microsoft Excel sheet, allowing a simple and fast analysis of VAWT during the design phase. The concept is based on multiple streamtube theory first developed in 1975 by Strickland [9]. This theory use Glauter's BEM theory and time average streamwise momentum equation to get the streamwise force. However, this model does not consider the local blade Reynold's Number and dynamic stall effects.

With the improvement of this limitation, Paraschivoiu [10] introduced multi-double streamtube model. In his model, induced velocity was taken as the average of the free stream and wake velocity. However, we found that it was impossible to obtain agreement between initially guessed induced velocity and the induced velocity from blade force in our Finite Phase Step Analysis in Excel. The use of blade forces resolved in the horizontal and vertical direction to obtain wake velocity is not satisfactory. In the current work, we use force on blade = change in air momentum

$$F_x = \dot{m}\left(V_\infty - V_{\text{wake, hori}}\right) \Rightarrow V_\infty - V_{\text{wake, hori}} = F_x/\dot{m}$$
$$F_y = \dot{m}\left(0 - V_{\text{wake, vert}}\right) \Rightarrow -V_{\text{wake, vert}} = F_y/\dot{m}$$

The obtained forces were used to calculate both upstream wake and downstream wake velocity.

Figures 1 to 6 show the resulting forces on a VAWT as determined by our Excel analysis using the asymmetrical S1223 airfoil. Figure 1 shows that when the blade is at an azimuth angle of 60 degrees, we note that the angle of attack at this condition is about 10 degrees, which should logically give a reasonable lift and without excessive drag. However, this is S1223 concave out configuration, where the experience lift coefficient is negative and negative torque is produced and it can be seen from Figure 7 where shows negative torque was generated.

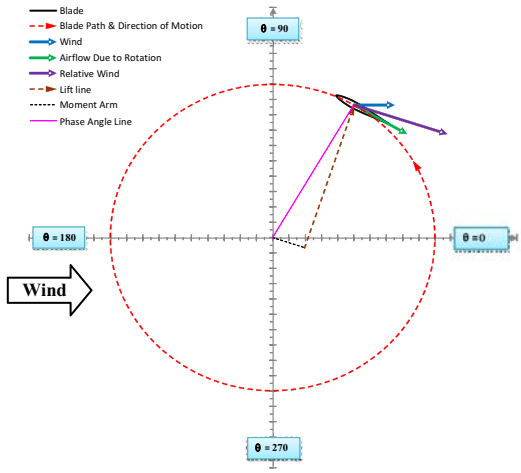

Figure 1: Torque diagram for θ = 60˚

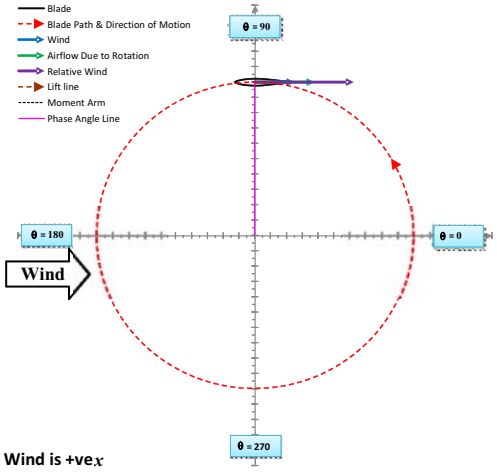

Figure 2: Torque diagram for θ = 90˚

As the blade rotates, it reaches at an azimuth angle of 90 degrees, it experiences a negative torque. The angle of attack at this angle is zero degrees. Thus the blade is produces negligible lift and experiences mainly drag. The corresponding torque can be viewed from Figure 7. It shows negative torque as well.

Rotating slightly from 90 degree, the line of action of lift (brown dashed arrow in Figure 3) has deviated slightly from the turbine axis and thus lift is able to provide torque due to the emergent lift moment arm (black dashed line in Figure 3). The drag on the blade is still present, and because of the much larger drag moment arm (represented by the length of the brown dashed arrow) the overall result is that the positive torque due to lift is approximately overcome by the negative torque due to drag.

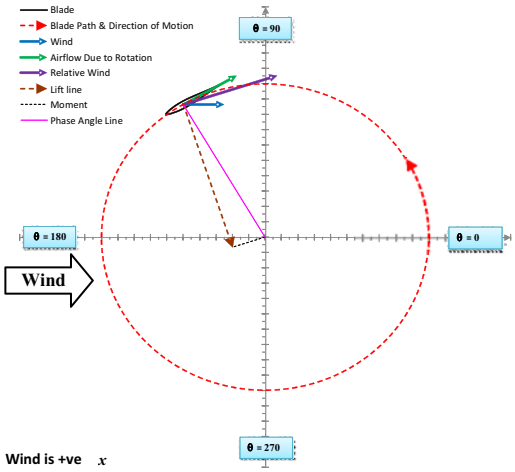

Figure 3: Torque diagram for θ = 120˚

The torque rises to almost maximum value at azimuth angle of about 120 degrees. Referring to Figure 3, this position corresponds an angle of attack of about 20 degrees, which is approximately the most optimum angle of attack. This position also results in a long lift moment arm length. At the same time, the drag moment arm length is reduced. Beyond azimuth angle of 120, the torque decreases until an azimuth angle of 180 degrees. At this position, the angle of attack is excessive, about 40 degrees, and the blade is badly stalled. So even while the lift moment arm is nearing its maximum length and the drag moment arm nearing its minimum, the poor lift to drag ratio of a stalled blade means that once again the positive lift torque is approximately overcome by the negative drag torque.

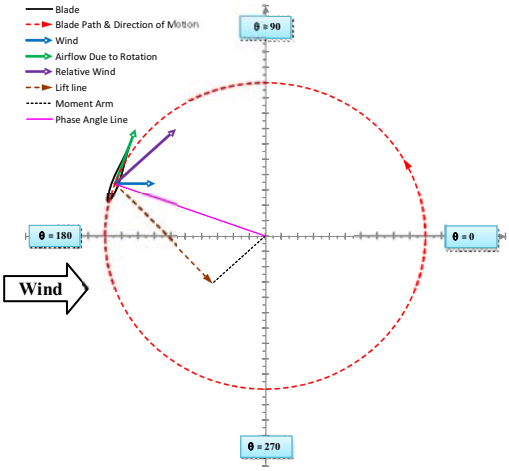

Figure 4: Torque diagram for θ = 160˚

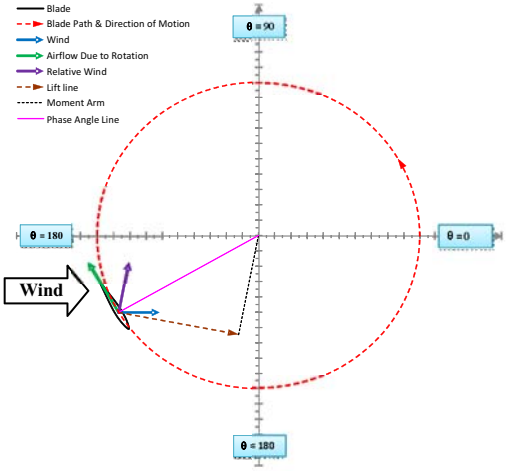

Figure 5: Torque diagram for θ = 210˚

From azimuth angle of 180 onwards, the torque is start to decrease mostly negative, with the exception of a small region from 180 to240 degrees shown in Figure 5. In this region, the angle of attack is again approximately at the most optimum value of about 20 degrees, as shown in Figure 5. However, the blade is now moving with the wind and thus the magnitude of the relative wind over the blade is low, resulting in low Reynolds number and hence poorer lift performance compared to the case when azimuth angle is 160 degrees.

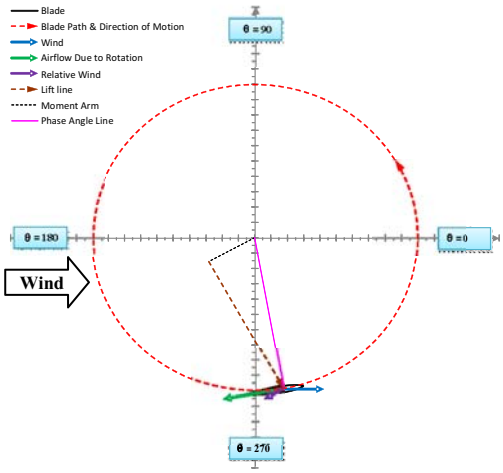

Figure 6: Torque diagram for θ = 280˚

In the remaining region of azimuth angle from 280 degree onwards, the wind interacting with the blade would have been affected by its earlier pass over an upstream blade and would not be perfectly horizontal nor close to the free stream wind speed. Thus the torque can only be more accurately predicted by simulation. However, a wind vector diagram of Figure 6 not gives an accurate prediction. For example, the simulation result show that the most negative torque occurs at azimuth angle of about 330 degrees.

The torque coefficient can be generated based on the overall analysis from above. The resulting performance curve

performed in the Excel sheet with Finite Phase Analysis can be found in Figure 7.

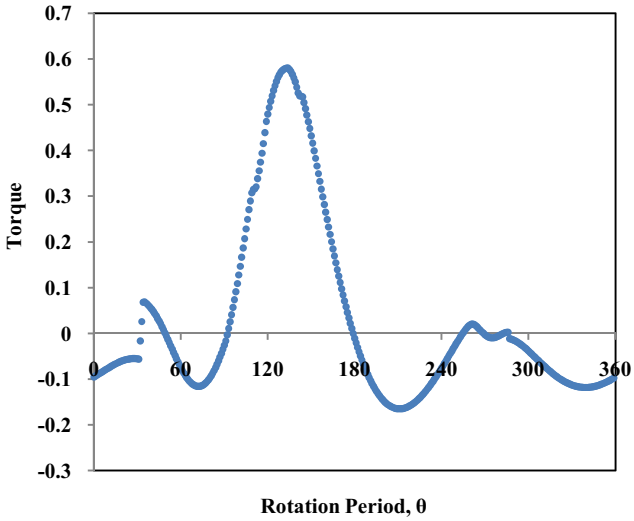

Figure 7: Generated torque coefficient by finite phase analysis in Excel.

3 VAWT Lab Model

Three different types of blade profiles were used for the study of the turbine performance. Much previous research on Darrieus – type VAWTs has employed NACA0012 [7], which shifted later to thicker airfoil NACA 0015 [11], NACA 0018 [12], and NACA 0022 [13]. Our investigation started with the study of airfoil NACA 0022 first for validation purpose. It was followed by the comparison of high lift curved blade S1223 and symmetric airfoil SD8020 with thicker airfoil NACA0022. The SD8020 airfoil was chosen, since this is a popular airfoil for low Reynolds numbers. The S1223 has shown to have high lift characteristics at low Reynolds-numbers. In order to study the self-starting capability of VAWT, the S1223 concave out configuration are tested here as well. All of the testing blade profiles were created with a thickness equal to its relative camber and a chord of 100mm. The blade span of 400mm (limited by the CNC foam cutter machine), gave the blades an aspect ratio of 4 and the turbine solidity (defined as sum of chord ÷ turbine diameter) value of 1.0. The layer of fibreglass was applied on the surface of the blade in order to improve its own strength and withstand the centrifugal bending force caused by the high rotational speeds of the turbine. The blades were attached on 200 mm long rotor arms resulting in a blockage ratio of 25% (based on turbine frontal swept area).

A small prototype of three and four-bladed configurations with different airfoil profile was studied and the performance efficiency and power output were compared. Figure 8 shows the overall dimension of the small scale turbine blade rotor. Four bladed prototype of small scaled vertical axis wind turbine and the model installed inside the wind tunnel testing section shown in Figure 9 and Figure 10. Wind tunnel measurements were obtained for cases of different wind velocity, tip speed ratio and different blade profile configurations.

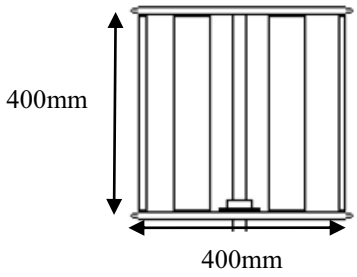

Figure 8 : Overall dimension of turbine blade rotor

Figure 9: Prototype of VAWT turbine model

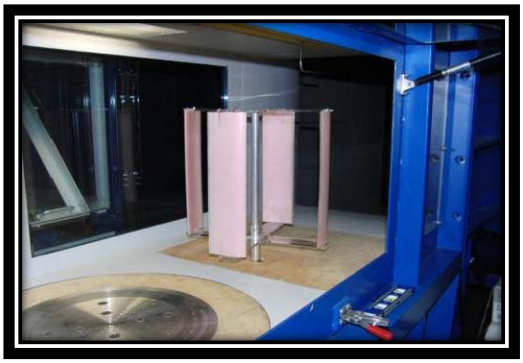

Figure 10: Model turbine display inside wind tunnel

Figure 11 shows the motoring, braking and torque measurement setup. The turbine shaft is supported by a bearing block (1) which contains two angular contact ball bearings arranged face-to-face. This combination of bearings provides effective support against axial and radial forces and moments. The lower end of the turbine shaft (2) is connected through a Huco Uni-Lat coupling (3) to an intermediate shaft (4). The Uni-Lat coupling allows both angular and radial misalignment. The intermediate shaft is supported by a self-aligning bearing block (5) which supports the shaft against axial and radial forces while allowing it to freely align itself

to the lower end of the turbine shaft. On this intermediate shaft is a set pulleys and timing belt (6) to transmit torque to an electromagnetic brake (7). The brake is a Placid Industries B6-24V. The ratio of number of teeth on the intermediate shaft to that on the brake is 1:2, i.e., the braking torque experienced by the intermediate shaft is half that of the brake's torque. The lower end of the intermediate shaft is attached to a 2-pole squirrel cage induction motor (8). The body of the motor and the brake are mounted on a frame (9). The other end of the frame is rigidly held by a torque sensor (10). The complete assembly is mounted on an aluminium profile frame (11) that is suspended from the outer floor of the wind tunnel test section (12).

The motor is controlled by a variable frequency inverter and it can be used in two ways: a) to motor the turbine to a high speed, b) to restrain the turbine to rotate at a desired speed. In case a), the turbine can be rotated to a speed higher than its maximum operating speed. Switching off the motor causes the turbine to slow down to its maximum operating speed. The brake can then be progressively increased to slow the turbine further for power measurement over a decreasing range of TSRs. In case b), the frequency applied to the motor can be maintained at a low value. The wind powers the turbine to rotate faster than the motor's synchronous speed. The motor thus operates with negative slip and provides a retarding torque and acts as a brake. The torque sensor shown in Figure 12 is the Chatillon STS-0050, with a measurement range of 0 to 5 Nm. The torque readings are manually read from the digital gauge DFS-R-ND. Rotating speed of the turbine is measured by an optical tachometer shining its spot of laser on a piece of reflective tape pasted on a convenient location on the turbine shaft.

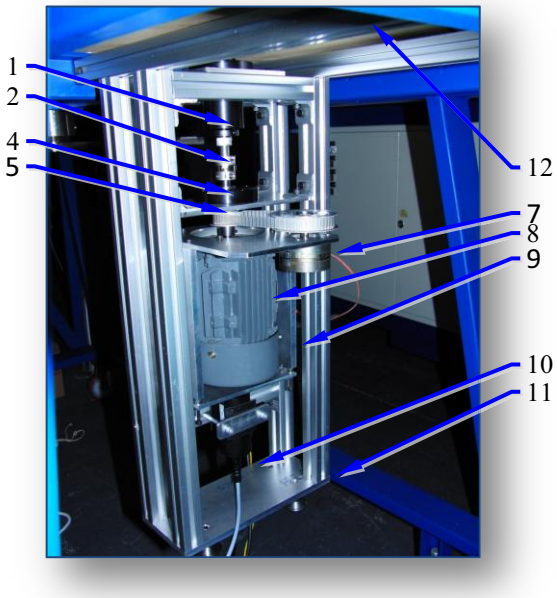

Figure 11: Support frame with motor, brake and torque sensor

The brake is controlled by a micro-controller. The duty cycle of the applied current is user-selectable in steps of 1%. When braking is applied, there is opposition to motion between its shaft and the body of the brake, i.e., the shaft does not turn easily, but slips with difficulty. This means that any torque applied to the shaft is transmitted to the body of the brake, via the frame and finally to the torque sensor. Hence the non-rotating torque sensor is able to measure the torque produced by the rotating turbine shaft. Wind speed at the most upstream end of the wind tunnel test section is measured by the pitot-static tubes of the wind tunnel.

Figure 12: Inverter and digital torque gauge

4 Wind Tunnel Results

The following section presents the results obtained from the wind tunnel measurements. The test was conducted at the Aerodynamics Laboratory at Nanyang Technological University (NTU) in Singapore. The low speed wind tunnel used for this study has test section dimensions of 720mm (H) x 780mm (W) x 2000mm (L). Figure 13 shows the self-staring capability of different blade profile, it shows that both NACA 0022 turbine configurations can self-start at low wind speed.

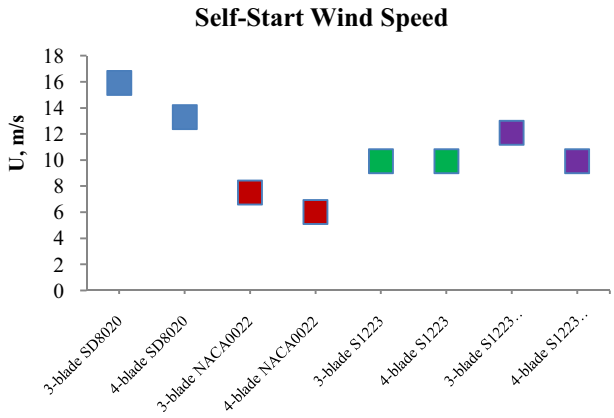

Figure 13: Self-starting capability of different blade profile

Figure 14 – Figure 17 show that the performance of wind tunnel measurements on 4 blades S1223 concave outward at wind speed 4.3m /s, 6m/s, 8 m/s and 10 m/s. It is noted that the performance curve of current blade profile cannot get a TSR beyond 2, the motor was used to speed up till its maximum speed, and however, the turbine slows down

once the motor is switched off. We then measure the torque and speed (RPM). We apply the brake to increase the torque gradually, recording speed and torque each time until the turbine stop. This gives the plot of the right hand side of the C_p vs. TSR curve

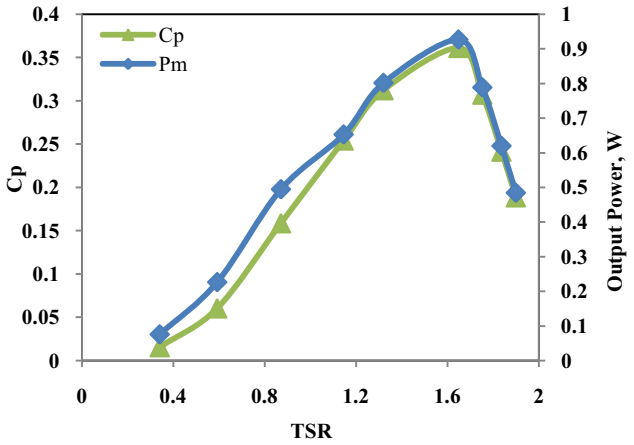

Figure 14 : performance of 4 blades S1223 concave outward configuration at wind speed 4.3 m/s

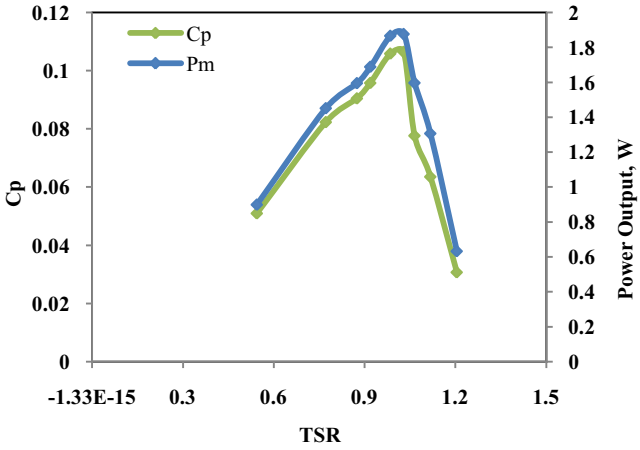

Figure 15: Performance of 4 blades S1223 concave outward configuration at wind speed 6m/s

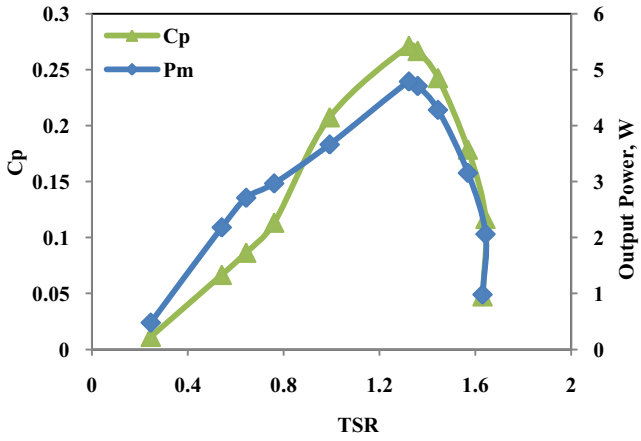

Figure 16 : performance of 4 blades S1223 concave outward configuration at wind speed 8 m/s

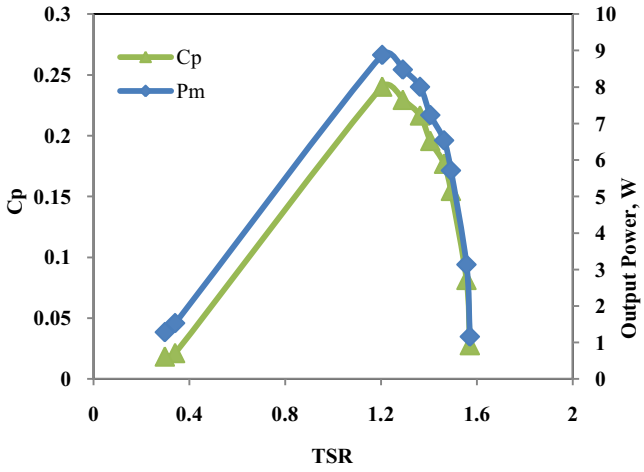

Figure 17: performance of 4 blades S1223 concave outward configuration at wind speed 10 m/s

To obtain the left hand side of the curve, we use the motor at low frequency to rotate the turbine at low speed. The wind pushes the turbine to rotate faster than the synchronous speed of the motor, thus the motor acts as a brake. We repeated with increasing motor frequency until the turbine accelerates beyond the peak power.

It is interesting to note that for a wind speed of 10 m/s (Figure 17), the performance curve has a sudden jump at the tip speed ratio 0.4.

5 Numerical Simulations and Comparison with Experimental Measurements

This section provides a comparison between the experimental measurements and the computational predictions carried out to get more fully understanding and the flow structure around the turbine model. The complexity of the unsteady aerodynamics of the VAWT makes it attractive for analysis with Computational Fluid Dynamics (CFD). The difficulty of the problem and the need for new design approaches for the VAWT have driven the focus of this research on the CFD modelling of the VAWTs to study the flow interaction with its blades during its rotation.

The geometry of the model is a representation of the wind tunnel experiment setup. Figure 18 shows the 2D grid and the sliding mesh that was used to model turbine motion. The commercial CFD code, ANSYS *Fluent* was used for numerical analysis. The model is bounded by two walls spaced 780mm apart, where the 250mm rotor radius with four-blades VAWT is placed. The rotor is represented by four blades of chord c=100 mm and 400 mm span, its axis is placed on the centre line of the tunnel test section, which is 140mm from the lower and top wall. The mesh was generated using the Gambit software included in the ANSYS Fluent

package, resulting in a 3D model with approximately 2 million cells in total (shown in Figure 18 and 19).

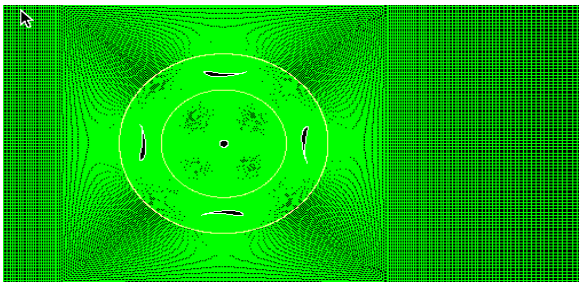

Figure 18 : Computational domain for 2D mesh generation

All simulation results presented in the current work refer to the revolutions of the rotor after periodic solutions were attained. The Unsteady Reynolds-averaged Navier-Stokes (URANS) equations govern the transport of the averaged flow quantities, with the whole range of the scales of turbulence being modelled. The RANS equations were solved using the green-gauss cell based gradient option and the sliding mesh method was used to rotate the turbine rotor blades. SIMPLEC algorithm was used for pressure-velocity coupling. The RNG k-epsilon model was adapted for the turbulence closure. Time integration was done implicitly and the minimum convergence criteria were set to 1e-06.

The entire 3D flow domain is shown in Figure 19 the boundary conditions were applied in order to solve the flow filed. The no-slip wall boundary condition was applied on the turbine blades, shaft surface and tunnel walls.

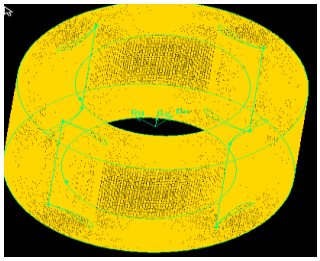

(a)

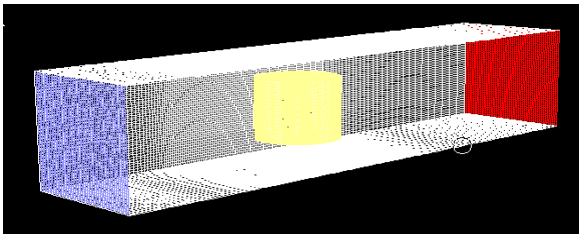

(b)

Figure 19: Computational domain (a) rotor blades area (b) three-dimensional simulation

5.1 Turbine Performance Prediction

This section presents all the comparison study among 2D, 3D simulation and finite phase analysis with Excel worksheet, which are arranged into three subsections. Section 5.1.1 shows 2D simulation results and the result compared with finite phase analysis, where 3D simulation and the difference to the 2D results shown in section 5.1.2. Detail turbine aerodynamic phenomena are presented in section 5.1.3

5.1.1 2D Computational Results

Figure 20 shows the torque predicted by the 2D simulation. The plot shows the torque coefficient for a wind speed of 6m/s at rotating speed 280rpm at tip seed ratio 1 and corresponding Reynolds number of 40,000. The plot shows that by far most of the torque is generated between Θ=120° to Θ=180°, when the blade is receiding in the wind.

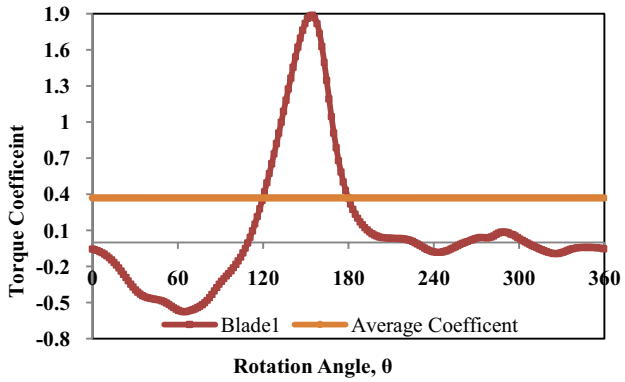

Figure 20: Torque coefficient prediction for a single rotating blade from 2D simulation at 280rpm

The comparison of torque between the 2D simulation and finite phase analysis is shown in Figure 21. We can see that the prediction of Finite Step Analysis follows a similar trend, but underpredicts the torque produced. We associate this difference due to the wall effect that is considered in 2D simulation,. For finite phase analysis, the sudden changes in the upstream and downstream velocity contribute at rotation angle 90, thus to make the whole torque curve a slightly different.

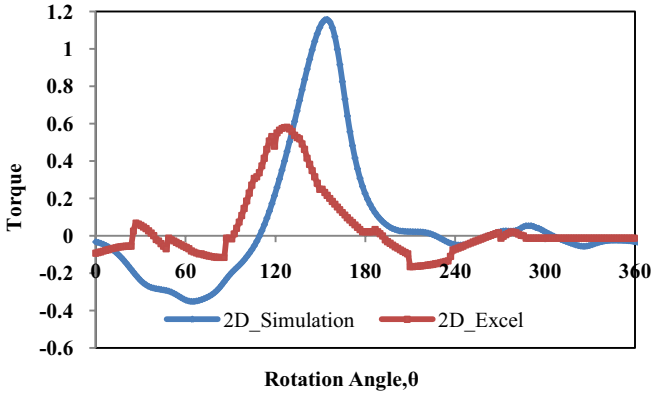

Figure 21: Comparison of torque prediction for a single blade between 2D simulation and finite phase analysis.

5.1.2 3D Computational Results

Comparisons of performance coefficient between 3D and 2D simulations of S1223 blade profile turbine model at wind speed 6m/s shown in Figure 22. While the 2D results over predict the power coefficient dramatically, the 2D simulations reproduce the trends observed in the 3D simulation giving hope that appropriate correction methods will allow to use 2D results for VAWT analysis.

Figure 23 shows the results for 3D simulations and experiments carried out for the turbine model at free wind speed 6m/s and corresponding Reynolds number 40,000. The 3D simulations are in good agreement with the experimental data with some small discrepancies. For example in Figure 23, the numerical results show an increased performance coefficient over the experimental measurement at a tip speed ratio of 1.1 which is mainly due to the strong wall effects with high rotating speed of the turbine rotor since the blockage effect is relatively large. On the other hand, the 3D simulations do not include the support arms. An additional drag force acting on the turbine may give reason for the lower performance from the experiment measurement.

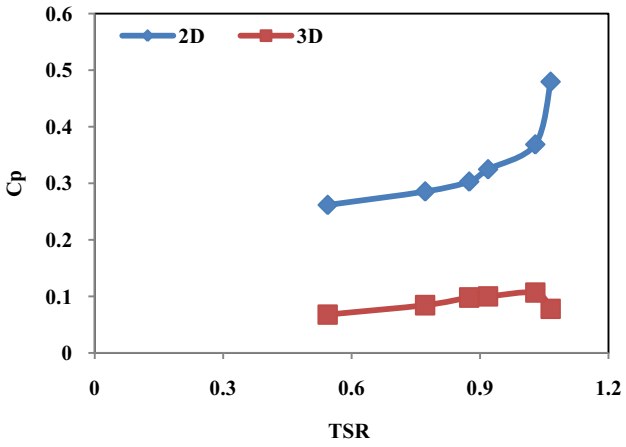

Figure 22: Comparisons of performance coefficient for the turbine model with 2D and 3D simulation at wind speed 6 m/s

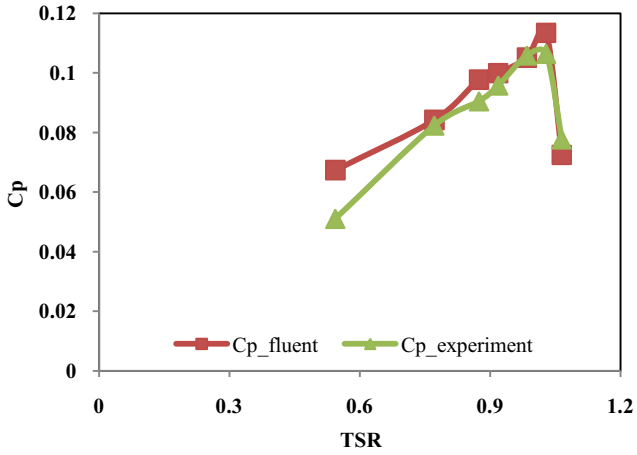

Figure 23: Comparisons of performance coefficient for the turbine model and 3D simulations at wind speed 6 m/s

The prediction of the torque coefficient from the equivalent 3D simulations is shown in Figure 24. While the overall shape of the curve for a single blade looks similar to that of the 2D simulation, the overall torque coefficient and average coefficient level has dropped dramatically compared with 2D simulation. We associate this mainly to the presence of the tip vortices.

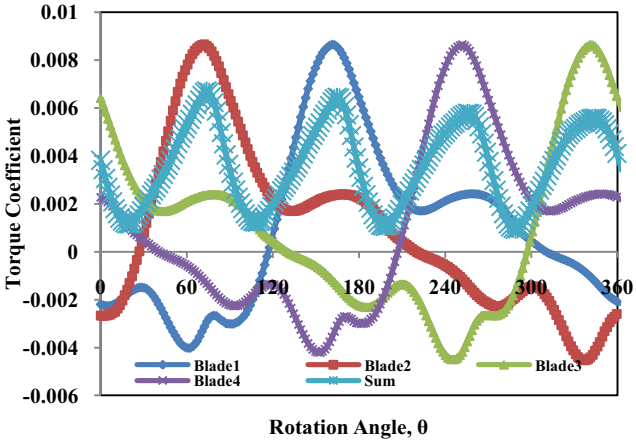

Figure 24: Torque coefficient prediction for overall turbine model from 3D simulation at 280rpm

Figure 25 compares the torque predicted by finite step analysis, 2D simulation and 3D simulation. We can see that the peak torque extracted in 3D simulation is lags about 20 degrees compared with 2D simulation and is substantially lower. Hence, the loss of torque needs to be found in the vortex structure of the flow field.

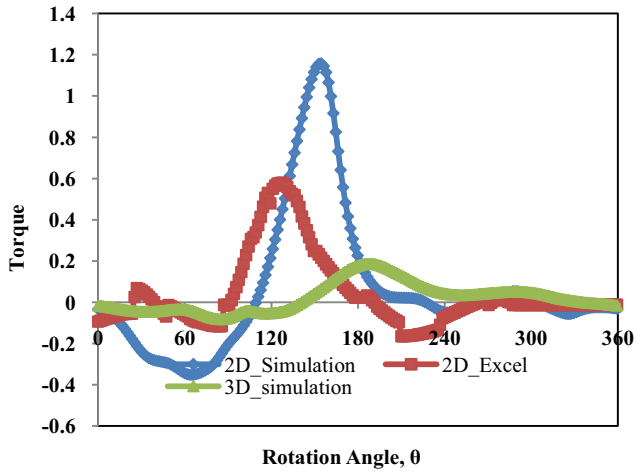

Figure 24: Comparison of torque between 2D, 3D simulation and 2D finite phase analysis with one blade

5.1.3 Detailed Vortex Structure of the Turbine

Vorticity isosurface (cf. Figure 26 and 27) generated from the 3D simulation results give more detailed insight into the complex flow phenomena. Figure 26 gives a general overview, while Figure 27 show the vortex structure at the receding blade at the instant of highest torque produced.

The variation of the blade tip vortex is due to the changing

lift and drag developed by the turbine rotor blade as it rotates through different phase angle. The vortex developed at the leading edge moves over the blade upper surface towards the tailing edge where it sheds off into the wake. It is very clear from the figure that the wake caused by the tip vortex extends to the area swept through by the other rotor blades. Moreover, it will also interact with the central shaft, as it is further travelling downstream.

Two main vortex structures can be identified. One is a dynamic leading edge vortex (A) that contributes to the lift and torque generated. The other is that of a wing tip vortex (B). In the four-blade configuration shown here, the wing tip vortices of the preceding blade are impinging on the torque generating blade at almost the exact moment, where the leading edge vortex is about to contribute to the torque. Hence, the flow on the torque generating blade is dramatically altered and is not able to produce the amount of torque predicted by 2D simulations.

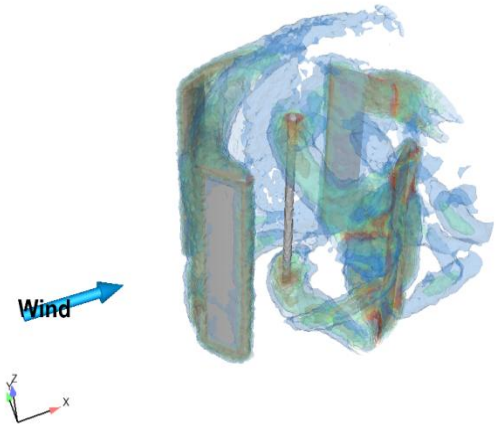

Figure 26 : Contour of vorticity for the four blades at different phase of 320 rpm 5 m/s

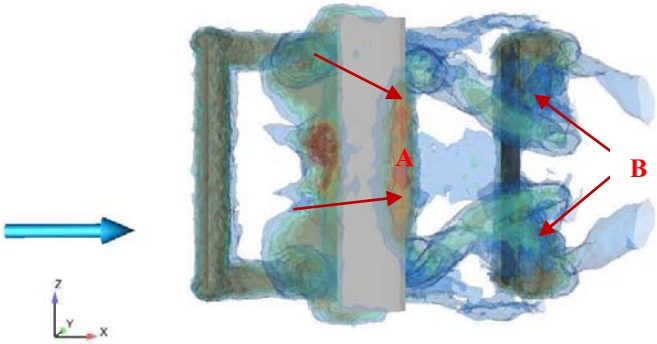

Figure 27 : Contour of vorticity for the four blades at different phase of 320 rpm 5 m/s

6 Conclusion

A small scale model of straight-bladed vertical axis wind turbine with different airfoil profiles has been developed and tested over a range of operating conditions. The straight bladed turbine rotor, with an aspect ratio of 4:1, operated at relatively very low tip speeds. The tunnel test results of staring wind characteristic show that the performance of the three tested airfoil profiles rank in the following order, highest performance first: 1) traditional NACA 0022 with thicker airfoil; 2) asymmetric airfoil S1223 with concave out configuration; 3) Symmetric airfoil SD8020. Numerical analysis of two and three dimensional unsteady flow field of straight bladed vertical axis wind turbine revealed significant influences of flow field on the upstream blade performance. This explains a relatively low wind power extraction potential when the blade is moving through the downstream azimuth angle. The three-dimensional CFD model captured interesting phenomena, such as blade tip vortices and support arm profile drags, in the VAWT operation. Significant difference are observed in the flow fields regarding the tip vortices, the wake from the supporting arms and shaft, which result in a significant reduction in the wind power extraction. Tests covering the full range of TSR have been conducted and the performance coefficients of S1223 concave out configuration give quite good results as well. We were especially able to obtain the c_p curve for low TSR. Comparison shows that 2D simulations over predict the results, but it show generally the same trend as experiments and 3D simulations. This allows to use 2D results in combination with models to compensate for 3D effects in order to analyze VAWT. Our 3D simulations show a more complete picture and we derive comparatively lower torque and performance due to finite wing effect. In future, then we will continue to develop low-order models for the design of VAWT based on our 3D models and experiments.

Acknowledgements

We thank the Energy Research Institute at NTU (ERI@N) for the support of the current work.

References

[1] B.K. Kirke, “Evaluation of Self-starting vertical axis wind Turbines for Stand-alone Applications”, PhD Thesis, Griffith University, Australia, (1998).

[2] D. Vandenberghe, E. Dick, “A free vortex simulation Method for Straight Bladed Vertical Axis Wind Turbine”, Journal of Wind Energy and Industrial Aerodynamics, 26, pp. 307-324, (1987).

[3] P. J. Musgrove, “Wind Energy Conversion: Recent Progress and Future Prospects”, Solar Wind Technology, 4, pp.37-49, (1987).

[4] E. Muljadi, K. Pierce, P. Migliore. “Control Strategy for Variable-speed, stall-Regulated Wind Turbines”, National Renewable Energy Laboratory, (1989).

[5] N. Fujisawa, S. Shibuya, “Observation of Dynamic Stall on Darrieus Wind Turbine Blades”, Journal of Wind

Energy and Industrial Aerodynamics, 89, pp.201-214, (2001)

[6] W.J. McCroskey, L.W. Carr, K.W. McAlister, "Dynamics Stall Experiments on Oscillating Airfoils. AIAA Journal, 14, pp. 57-63, (1976)

[7] M.T. Brahimi, A. Allet, I. Paraschivoiu, "Aerodynamic Analysis Model for Vertical Axis Wind Turbines", International Journal of Rotating Machinery, 2, pp. 15-21, (1995).

[8] I.S. Hwang, S.Y. Min, I.O. Jeong, Y.H. Lee, S.J. Kim, "Efficiency Improvement of a New Vertical Axis Wind Turbine by Individual Active Control of Blade Mition", School of Mechanical and Aerospace Engineering, Seoul National University, the Republic of Korea.

[9] R.J. Strickland. "A Performance Prediction Model for the Darrieus wind Turbine". International Symposium on Wind Energy Systems, Cambridge, UK, pp. C3-39-54, (1976).

[10] I. Paraschivoiu. "Double-Multiple Streamtube model for Darrieus Wind Turbines. Second DOE/NASA Wind Turbines Dynamics Workshop, NASA CP-2186, pp.19-25, (1981).

[11] M. Marini, A Massardo, A. Satta. "Performance of Vertical Axis Wind Turbine with Different Shapes", Journal of Wind Energy and Industrial Aerodynamics, 39, pp. 83-93, (1992).

[12] O. Agren, M. Berg, M. Lejion. "A Time-dependent Potential Flow Theory for a Aerodynamics of Vertical Axis Wind Turbines", Journal of Applied Physics, 97, (2005).

[13] R. Howell et al. "Wind Tunnel and Numerical Study of a Small Vertical Axis Wind Turbine", Journal of Renewable Energy, 35, pp. 412-422, (2010).